Live imaging YAP signaling *in vivo* with fusion reporter mice

Authors

Bin Gu[1,7,8*#], Brian Bradshaw[1*], Min Zhu[1,2,3*], Yu Sun[3,4,5], Sevan Hopyan[1,2,6], and Janet Rossant[1,2#]

Affiliations:

[1] Program in Developmental and Stem Cell Biology, Hospital for Sick Children, Toronto, ON M5G 0A4, Canada.

[2] Department of Molecular Genetics, University of Toronto, Toronto, ON M5S 1A8, Canada.

[3] Department of Mechanical and Industrial Engineering, University of Toronto, Toronto, ON M5S 3G8, Canada;

[4] Institute of Biomaterials and Biomedical Engineering, University of Toronto, Toronto, ON M5S 3G9, Canada;

[5] Department of Electrical and Computer Engineering, University of Toronto, Toronto, ON M5S 3G4, Canada

[6] Division of Orthopaedic Surgery, The Hospital for Sick Children, University of Toronto, Toronto, ON M5G 1X8, Canada;

[7] Present Address: Department of Obstetrics, Gynecology and Reproductive Biology, Michigan State University, East Lansing, MI 48824, USA

[8] Present Address: Institute for Quantitative Health Science and Engineering, Michigan State University East Lansing, MI 48824, USA

*Equal contribution #Correspondence to Janet Rossant (janet.rossant@sickkids.ca) and Bin Gu (gubin1@msu.edu)

Abstract:

YAP protein is a critical regulator of mammalian embryonic development. By generating a near-infrared fusion YAP reporter mouse line, we have achieved high-resolution live imaging of YAP localization during mouse embryonic development. We have validated the reporter by demonstrating its predicted responses to blocking Lats kinase activity or blocking cell polarity. The YAP fusion reporter mice and imaging methods will open new opportunities for understanding dynamic YAP signaling *in vivo* in many different situations.

Main text:

Yes associated protein 1 (Yap1)-commonly referred to as YAP protein, is a signaling protein that serves as a hub of biochemical and mechanical sensing[1-3]. YAP plays crucial regulatory roles in enormously diverse processes in development and disease, from the very beginning of life, such as mammalian preimplantation development[4], to the very late stage of disease, such as cancer metastasis[5]. Real-time tracking of the dynamic YAP signaling status *in vivo* would offer crucial insights into the fundamental regulatory mechanisms of mammalian development and disease.

YAP is a transcriptional co-activator for the TEA domain (TEAD) family transcription factors[6]. In response to numerous signals, YAP shifts its sub-cellular distribution to the nucleus where it associates with TEAD proteins to activate gene expression. Thus, monitoring the nuclear/cytoplasmic localization of YAP is the most broadly applied method to evaluate YAP activity[6,7]. Currently, this is primarily achieved by immunostaining of fixed embryos or tissue sections, precluding the acquisition of dynamic information. Although live imaging has been achieved in Drosophila and human cell lines and revealed

intriguing YAP behaviours[8,9], no appropriate tools exist for live imaging endogenous YAP protein in mammals *in vivo*.

We set out to engineer a knock-in (KI) fusion reporter of *Yap* in mice (Extended Figure 1). There have been several previous attempts to generate endogenous *Yap* KI reporters, including by ourselves, without success. The function of mammalian YAP seems to be easily disrupted by fusion tags. We tested different combinations of tagging position and linker sequences and finally successfully generated a healthy reporter mouse line by C-terminal tagging with a long (30 amino acid) flexible linker (Extended Figure 1A). Other designs, such as N-terminal tagging with the same linker led to embryo death at embryonic days 8.5 (E8.5), similar to Yap knockout embryos, suggesting functional interference[10]. To allow good light penetration for imaging deep tissue layers in postimplantation mammalian embryos and other tissues, we chose to use a bright near-infrared (NIR) fluorescent protein (FP), enhanced miRFP670(emiRFP670), as the fluorescent indicator[11]. We performed extensive quality control to confirm single-copy insertion of the fusion reporter with the correct sequence, as detailed in online methods and extended Figure 1B and our published protocol[12,13]. The homozygous mice are healthy and fertile. The mouse line was maintained in the homozygous state after outcrossing for 5 generations to ensure no carry-over of any possible off-target alterations.

We validated the reporter in mouse preimplantation embryos where the YAP distribution and its responses to various interventions are well characterized. The nuclear/cytoplasmic distribution of YAP from 8-cell stage onward is well established from previous research: At 8-cell stage, all blastomeres have nuclear localized YAP. From 16-cell stage to early-mid blastocyst stage (E3.5), nuclear YAP is restricted to the outer cells

that will give rise to the trophectoderm[7]. By the expanded blastocyst stage (E4.5), some epiblast cells will start to present nuclear YAP status[14]. Our live imaging reproduced this pattern (Figure 1A). Before the 8-cell stage, the localization of YAP distribution is more debatable. Our live imaging showed that YAP was evenly distributed in the cytoplasm and nucleus of blastomeres until the early 4-cell stage, at which point YAP begins to be more restricted to the nucleus (Figure 1A). We further validated the colocalization of the C-YAP reporter with the endogenous YAP protein and with the expression of CDX2 protein in the TE of blastocysts by immunofluorescence (Figure 1B). Then we investigated whether the C-YAP reporter protein can respond appropriately to exogenous signals. In mouse early embryos, YAP localization is controlled by HIPPO and polarity signaling pathways. From the HIPPO signaling pathway, LATS1/2 kinase is responsible for the phosphorylation of YAP, which leads to its sequestration in the cytoplasm[7]. Overexpressing a kinase-dead LAT kinase (dnLATS2) can promote the nuclear localization of YAP and the expression of CDX2 even in inside cells[7]. This result was replicated when we injected a dnLATS2 mRNA into homozygous C-YAP embryos (Figure 1C). As for polarity, it has been shown that the inhibition of the Rho-associated protein kinase (ROCK) kinase using a small molecular inhibitor Y27632 resulted in universal cytoplasmic YAP localization, and as a result, failure to establish the TE[15]. We cultured C-YAP reporter embryos from 8-16 cell stages in Y27632 and live imaged them. As shown in Figure 1D and movie 1, ROCK inhibition indeed resulted in a cytoplasmic YAP localization in all cells (Figure 1D).

We then used the validated reporter mouse line to analyze the behaviour of YAP during embryonic development in real-time. A key event that YAP regulates during

preimplantation development is the initiation of inner cell mass (ICM)- TE segregation at the 16-cell stage. When 8-cell embryos transition to 16-cell embryos through cell division, YAP becomes localized in the nucleus of blastomeres located on the surface of the embryos (outside cells) and excluded from the nucleus in inside cells[7]. The presence of nuclear YAP drives the expression of the TE-specific transcription factor CDX2 in outside cells, initiating TE lineage differentiation. In contrast, the enclosed blastomeres with cytoplasmic localized YAP initiate *Sox2* expression and ICM differentiation[16]. However, the exact process that leads up to this asymmetric YAP signaling status is still debatable. Some models suggest a fixed determination of YAP localization at the time of generation of inside and outside 16-cell blastomeres, while other recent studies suggesting a more dynamic process[17,18]. Direct observation of the YAP dynamics through the 8-16 cell stage is the best way to resolve these models.

We time-lapse imaged homozygous C-YAP reporter embryos every 20 mins at the transition between the 8-cell to 16-cell stage for a period of 20 hours. Cell nuclei were marked by a live DNA dye (Movies 2-3, with additional movie from 4-cell stage-Movie 4). To rule out the possibility of the imaging process affecting normal development, we further cultured the embryos to E4.5 and validated a high blastocyst formation rate (8/9) (Extended Figure 2A). The movies revealed profound dynamic movements of blastomeres in 8-16 cell stage embryos. Many cells changed their relative outside-inside position from where they were localized right after the cell division that generates them (Movies 2 and 3). We discovered an intriguing dynamic behavior pattern of YAP during this transition through closer inspection and tracking cells from the movies. When an 8-cell blastomere divides to form two daughter cells - 16-cell blastomeres, both always show

nuclear localization of YAP, regardless of the direction of the cell division axis (Figure 2A). It took roughly 100-300 mins for the two daughter cells to adopt their final position in the embryo (Figure 2A). The final position that a cell adopted determined its YAP distribution- when a cell adopted an outside position, it presented nuclear YAP, whereas when a cell adopted an inside position, it presented cytoplasmic YAP (Examples in Figure 2A and quantifications in Extended Figure 2B and C). There was an almost equal chance for two 16-cell blastomeres from a single 8-cell blastomere to adopt one of the two relative positions – outside-outside or outside-inside (Extended Figure 2D). A previous report has suggested that a significant proportion of inside cells at the 16-cell stage are the result of cell movement rather than oriented cell division, consistent with our observations[18]. The C-YAP reporter allowed us to relate this dynamic cell movement to a dynamic regulation of YAP signaling, which could further lead to cell lineage determination. Interestingly, the movie of embryos treated with ROCK inhibitor showed that (Movie 1 and 5 and Figure 2B), although ROCKi eventually inhibited YAP nuclear localization in all 16-cell blastomeres, the initial YAP nuclear localization right after cell division was not affected, suggesting a differential involvement of ROCK-related processes, such as polarity and mechanical tension, in regulating these two distinct YAP nuclear localization processes. How this dynamic behavior is controlled remains an open question, which can now be addressed by live imaging the YAP reporter model in combination with additional KI reporters tracking polarity and mechanical tension.

Preimplantation embryos are small and transparent. To demonstrate the broader application of the YAP reporter in more challenging samples, we live-imaged C-Yap embryos at E8.0 (before turning, Movie 6), E8.5 (after turning, Movie 7), and E9.5 (Movie

8) using light-sheet imaging technology. We achieved high resolution imaging of multiple tissues including those located in deep tissue layers (up to 200μm), such as the heart tube (Extended Figure 3B-D and z stack in movie 9). In most regions, tissues consisted primarily of cells with cytoplasmic YAP, with only small populations of cells with strong nuclear signals (extended Figure 3 B-D, examples marked by arrows). In the heart tube, on the other hand, most cells showed nuclear YAP which may be consistent with the mechanical load these cells are subjected to and suggests a crucial role for YAP in heart development[19,20]. Time lapse imaging of E8.5 embryos every 5 mins for 3 hours (Movies 10) revealed a population of cells with strong nuclear YAP signal migrating within the head region. The identity of these cells warrants further investigation. These data demonstrate that the C-YAP reporter can have broad imaging applications in challenging samples such as late-stage embryos and tissues.

In summary, we present the first KI fusion reporter mouse model to enable the readout of YAP nuclear-cytoplasmic localization by live imaging. Using this line, we reveal new aspects of dynamic YAP behaviour in preimplantation mouse embryos and the capacity to live-image postimplantation embryos with penetration at depths of up to 200μm. This live imaging YAP reporter can be combined with other appropriate reporters to study multiple developmental and disease processes.

Methods:

Designs of guide RNAs and knock-in repair donors:

As described before, a guide RNA target spanning the Stop TAG codon: TCACGTGGTTATAGAGCTGC**AGG** were selected using the CRISPOR algorism (http://crispor.tefor.net) based on specificity scores[21]. The chemically modified single guide RNAs (sgRNAs) of with the sequence of UUGCGCGGGCUCCAUGGCUG were synthesized by Synthego Inc. Similar to previously described, the repair donor for C-YAP reporter were designed as illustrated in Extended Figure 1A. The emiRFP670 and the linker coding sequences in proper orientation were flanked by long homology arms (813bp 5' arm and 717bp 3'arm) on each side and replacing the stop codon of the *Yap1* gene. The Donor DNA sequence was synthesized by Epoch Life Science (http://www.epochlifescience.com) and cloned into a PBSK plasmid backbone.

Generating KI reporter mouse lines by 2C-HR-CRISPR:

The KI reporter mouse line was generated following our published protocol using 2C-HR-CRISPR on the CD1 background[13,22]. Briefly, Cas9 monomeric streptavidin (mSA) mRNAs were produced by in vitro transcription using the mMessage mMachine SP6 Kit (Thermo Scientific). PCR templates were generated by PCR reaction with biotinylated primers using high fidelity ClonAmp HiFi PCR mix (Takara Inc.). A mixture of Cas9-mSA mRNA (75ng/μl), sgRNA (50ng/μl), and biotinylated repair donor (20ng/μl) was microinjected into the cytoplasm of 2-cell stage mouse embryos and transferred same day to pseudo-pregnant females. Founder pups were obtained from the pregnancies.

We established founder mice with correct insertion at high efficiency (2/2 live born pups-100% efficiency). A founder was crossed five generations to wildtype CD1 mice to breed out any potential off-target mutations introduced by CRISPR-Cas9 and then bred to

homozygote at N6 generation. The mouse line is then kept as homozygotes. In the early generations of homozygous breeding, a cataract phenotype was observed in some mice. This phenotype was then removed by selectively breeding C-YAP homozygous reporter mice without such a phenotype. The homozygous mice are otherwise healthy and fertile without apparent phenotype.

Genotyping and genetic quality controls:

Founder mice were genotyped by PCR amplification with primers spanning homology arms using the following primers: 5' arm gtF: GTTCTAAGGTAGACACTGTGTGCTTCAGTT and 5'arm gtR: TCATGTTCGCAGGTCAAGAGGTCA; 3'arm gtF: CTGGTTGTCTGTCACCATTATCTGC and 3'arm gtR: AACACCTGCAATTGCTCCAACC. Founder mice were out-crossed to CD1 mice to generate N1 mice. The N1 mice were genotyped by PCR. Additionally, genomic regions spanning the targeting cassette and 3' and 5' homology arms were Sanger-sequenced to validate correct targeting and insertion copy number was evaluated by droplet digital PCR (performed by the Centre for Applied Genomics at the Research Institute of The Hospital for Sick Children, Toronto). Heterozygous N1 mice have only one insertion copy, demonstrating single copy insertion. All animal work was carried out following the Canadian Council on Animal Care Guidelines for Use of Animals in Research and Laboratory Animal Care under protocols approved by the Centre for Phenogenomics Animal Care Committee (20-0026H).

Embryo isolation, culture, and treatments:

Preimplantation embryos were isolated from superovulated females that were bred to males, both homozygous for the C-YAP reporter. Embryos are isolated from oviducts or

uterus at appropriate stages appropriate to each experiment – E0.5 for zygote, E1.5 for 2-cell embryos, E2.5 for 8-cell embryos and E3.5 for blastocysts as previously described. Embryos were flushed with M2 medium. They were then cultured in small drops of KSOM-AA medium under mineral oil at 37°C, with 6% CO2 for specified times. For the Rock inhibitor treatment experiment, 8-cell stage embryos were cultured in KSOM-AA medium supplemented with 20μM Y-27632.

Live imaging preimplantation embryos:

For imaging the YAP dynamics during the formation of 16-cell embryos, embryos were flushed from the oviduct at 8-cell or 4-cell stage and cultured in a 3ul drop of KSOM-AA medium under mineral oil on a MatTek glass bottom dish. Live imaging was performed at 20mins/frame for 24-36 hours. For the ROCKi inhibitor treatment, embryos were flushed from the oviduct at 8-cell stage and cultured in a 3ul drop of KSOM-AA medium with 20μM Y-27632 under mineral oil on a MatTek glass-bottom dish. Live imaging was performed every 90 mins for 24 hours.

dnLAT2 mRNA injection:

Homozygous YAP-C embryos were collected at 2-cell stage. mRNAs were microinjected into one of the two blastomeres as previously described. For control experiments, embryos were injected with H2B-RFP mRNAs at 300ng/μl. Treatment embryos were injected with dnLats2 1000ng/μl plus H2B-RFP 300ng/μl. The embryos were then cultured to the early blastocyst stage for immunofluorescent analysis.

Whole-mount immunofluorescent staining of embryos

Whole mount immunofluorescent staining of embryos was performed as previously described[23]. Briefly, embryos were fixed in 4% paraformaldehyde at room temperature for

15 minutes, washed once in PBS containing 0.1% Triton X-100 (PBS-T), permeabilized for 15 minutes in PBS 0.5% Triton X-100 and then blocked in PBS-T with 2% BSA (Sigma) and 5% normal donkey serum (Jackson ImmunoResearch Laboratories) at room temperature for 2 hours, or overnight at 4°C. Primary and secondary antibodies were diluted in blocking solution, staining was performed at room temperature for ~2 hours or overnight at 4°C. Washes after primary and secondary antibodies were done three times in PBS-T. Nuclear staining was performed using Hoechst 33258 (Thermo scientific) at a concentration of 10µg/ml for 20 minutes at room temperature. Embryos were mounted in PBS in wells made with Secure Seal spacers (Molecular ProbesTM, Thermo Fisher Scientific) and placed between two cover glasses for imaging. Primary antibodies: Goat anti-tdTomato (Biorbyt orb182397 Lot AR2150) at 1:200 dilution, Rabbit anti YAP (Cell Signalling Technology (D8H1X) XP Ref 11/2018 Lot4) at 1:100 dilution and Mouse anti Cdx2(Biogenex MU392A-UC Lot MU392A0714) at 1:100 dilution. Secondary antibodies all from Themo Scientific and at 1:400 dilusion: Donkey-anti-goat IgG AF 546 (A11056 Lot 1714714), Donkey anti Rabbit IgG AF647(A31573 Lot 1693297) and Donkey anti mouse IgG AF488 (A21202 Lot 1741782)

Confocal imaging of preimplantation embryos:

Both live and immunostained images of preimplantation embryos were acquired using a Zeiss Axiovert 200 inverted microscope equipped with a Hamamatsu C9100-13 EM-CCD camera, a Quorum spinning disk confocal scan head, and Volocity acquisition software version 6.3.1. Single plane images or Z-stacks (at 1µm intervals) were acquired with a 40x air (NA=0.6) or a 20x air (NA=0.7) objective. Images were analyzed using Volocity

software. Live imaging was performed in an environment controller (Chamlide, Live Cell Instrument, Seoul, South Korea) on the same microscope.

Time-lapse imaging was performed on the same microscope equipped with an environment controller (Chamlide, Live Cell Instrument, Seoul, South Korea). Embryos were placed in a glass-bottom dish (MatTek) in KSOM-AA covered with mineral oil. A 20x air (NA=0.7) objective lens was used. Images were acquired at 1-3μm Z intervals with time-lapse settings as indicated in figure legends.

Lightsheet imaging of post-implantation embryos:

Three-dimensional time-lapse microscopy was performed on a Zeiss Lightsheet Z.1 lightsheet microscope. Embryos were suspended in a solution of DMEM without phenol red containing 12.5% filtered rat serum and 1% low-melt agarose (Invitrogen) in a glass capillary tube. Once the agarose solidified, the capillary was submerged into an imaging chamber containing DMEM without phenol red, and the agarose plug was partially extruded from the glass capillary tube until the portion containing the embryo was completely outside of the capillary. The temperature of the imaging chamber was maintained at 37° C with 5% CO2. Images were acquired using a 20× objective with dual-side illumination in a multi-view mode (4 evenly spaced views spanning 360° for E8.0 embryos imaging) or tile scanning mode (for E8.5 and E9.5 embryos imaging). Images were acquired for 3 hours with 5 min. intervals. The light sheet images were processed using Zen (Zeiss), Arivis Vision4D (Arivis), Imaris (Bitplane) and ImageJ.

Imaging quantification analysis:

Preimplantation images were visualized using the Volocity 6.3 software. The live images of preimplantation embryos were traced manually by carefully inspect the movie with cell

nucleus marked by the live DNA dye and the C-YAP reporter. For quantifying fluorescent intensity, images were exported as TIFF files and measured using the Region of interest (ROI) function in ImageJ 1.53a software. The average fluorescent intensity of each nuclear ROI was measured and subtracted a general background fluorescent intensity in the correspondent image.

Statistics:

Statistics on numerical data were performed using the Prism 9 software(GraphPad Software, LLC.). For intergroup comparison, the data were first subjected to the D'Agostino & Pearson normality test. Datasets that conform to a normal distribution were then subjected to the unpaired Student's-t test, and the ones does not conform to a normal distribution were then subjected to the Mann Whitney test. 2-tailed analysis were used in all cases. Exact p-values were presented in the figures. For the one group t-test for the proportion of relative position of cell division pairs at 16-cell stage, a null hypothesis of the proportion= 50% were tested against and resulted in a p-value (p=0.0381).

Acknowledgement:

This work was funded by CIHR (FDN-143334) to J.R CIHR (MOP 168992) to S.H and Y.S, and Medicine by Design Grand Questions Program (Canada First Research Excellence Fund) to S.H and Y.S. The authors acknowledge technical support from the Model Production Core staff led by M. Gertsenstein at the Centre for Phenogenomics; E. Posfai (Princeton University) for early collaboration efforts on generating an N-terminal Halo-tagged YAP reporter; V. Verkhusha (Albert Einstein College of Medicine) for

providing a construct encoding the emiRFP670 fluorescent protein and discussions on selecting NIR fluorescent proteins.

Data Availability Statement:

The raw data that support the findings of this study are available from the corresponding authors on reasonable request.

Author contributions

B.G., and J.R. conceived the study. B.G. designed and produced the C-YAP reporter mouse line. B.G , B.B and M.Z designed, carried out and analyzed all experiments. J.R., Y.S and S.H. provided supervision and funding for the study. B.G and J.R wrote the manuscript and all authors reviewed and approved the manuscript.

Competing Financial Interest

Authors declare no competing financial interests.

References:

1 Ma, S., Meng, Z., Chen, R. & Guan, K. L. The Hippo Pathway: Biology and Pathophysiology. *Annu Rev Biochem* **88**, 577-604, doi:10.1146/annurev-biochem-013118-111829 (2019).

2 Panciera, T., Azzolin, L., Cordenonsi, M. & Piccolo, S. Mechanobiology of YAP and TAZ in physiology and disease. *Nat Rev Mol Cell Biol* **18**, 758-770, doi:10.1038/nrm.2017.87 (2017).

3 Zheng, Y. & Pan, D. The Hippo Signaling Pathway in Development and Disease. *Dev Cell* **50**, 264-282, doi:10.1016/j.devcel.2019.06.003 (2019).

4 Rossant, J. Genetic Control of Early Cell Lineages in the Mammalian Embryo. *Annu Rev Genet* **52**, 185-201, doi:10.1146/annurev-genet-120116-024544 (2018).

5 Thompson, B. J. YAP/TAZ: Drivers of Tumor Growth, Metastasis, and Resistance to Therapy. *Bioessays* **42**, e1900162, doi:10.1002/bies.201900162 (2020).

6 Zhao, B. *et al.* TEAD mediates YAP-dependent gene induction and growth control. *Genes Dev* **22**, 1962-1971, doi:10.1101/gad.1664408 (2008).

7 Nishioka, N. *et al.* The Hippo signaling pathway components Lats and Yap pattern Tead4 activity to distinguish mouse trophectoderm from inner cell mass. *Dev Cell* **16**, 398-410, doi:10.1016/j.devcel.2009.02.003 (2009).

8 Manning, S. A. *et al.* Dynamic Fluctuations in Subcellular Localization of the Hippo Pathway Effector Yorkie In Vivo. *Curr Biol* **28**, 1651-1660 e1654, doi:10.1016/j.cub.2018.04.018 (2018).
9 Franklin, J. M., Ghosh, R. P., Shi, Q., Reddick, M. P. & Liphardt, J. T. Concerted localization-resets precede YAP-dependent transcription. *Nat Commun* **11**, 4581, doi:10.1038/s41467-020-18368-x (2020).
10 Morin-Kensicki, E. M. *et al.* Defects in yolk sac vasculogenesis, chorioallantoic fusion, and embryonic axis elongation in mice with targeted disruption of Yap65. *Mol Cell Biol* **26**, 77-87, doi:10.1128/MCB.26.1.77-87.2006 (2006).
11 Matlashov, M. E. *et al.* A set of monomeric near-infrared fluorescent proteins for multicolor imaging across scales. *Nat Commun* **11**, 239, doi:10.1038/s41467-019-13897-6 (2020).
12 Gu, B., Gertsenstein, M. & Posfai, E. Generation of Large Fragment Knock-In Mouse Models by Microinjecting into 2-Cell Stage Embryos. *Methods Mol Biol* **2066**, 89-100, doi:10.1007/978-1-4939-9837-1_7 (2020).
13 Gu, B., Posfai, E. & Rossant, J. Efficient generation of targeted large insertions by microinjection into two-cell-stage mouse embryos. *Nat Biotechnol* **36**, 632-637, doi:10.1038/nbt.4166 (2018).
14 Hashimoto, M. & Sasaki, H. Epiblast Formation by TEAD-YAP-Dependent Expression of Pluripotency Factors and Competitive Elimination of Unspecified Cells. *Dev Cell* **50**, 139-154 e135, doi:10.1016/j.devcel.2019.05.024 (2019).
15 Kono, K., Tamashiro, D. A. & Alarcon, V. B. Inhibition of RHO-ROCK signaling enhances ICM and suppresses TE characteristics through activation of Hippo signaling in the mouse blastocyst. *Dev Biol* **394**, 142-155, doi:10.1016/j.ydbio.2014.06.023 (2014).
16 Wicklow, E. *et al.* HIPPO pathway members restrict SOX2 to the inner cell mass where it promotes ICM fates in the mouse blastocyst. *PLoS Genet* **10**, e1004618, doi:10.1371/journal.pgen.1004618 (2014).
17 Zhang, H. T. & Hiiragi, T. Symmetry Breaking in the Mammalian Embryo. *Annu Rev Cell Dev Biol* **34**, 405-426, doi:10.1146/annurev-cellbio-100617-062616 (2018).
18 Watanabe, T., Biggins, J. S., Tannan, N. B. & Srinivas, S. Limited predictive value of blastomere angle of division in trophectoderm and inner cell mass specification. *Development* **141**, 2279-2288, doi:10.1242/dev.103267 (2014).
19 Lindsey, S. E., Butcher, J. T. & Yalcin, H. C. Mechanical regulation of cardiac development. *Front Physiol* **5**, 318, doi:10.3389/fphys.2014.00318 (2014).
20 Zhou, Q., Li, L., Zhao, B. & Guan, K. L. The hippo pathway in heart development, regeneration, and diseases. *Circ Res* **116**, 1431-1447, doi:10.1161/CIRCRESAHA.116.303311 (2015).
21 Concordet, J. P. & Haeussler, M. CRISPOR: intuitive guide selection for CRISPR/Cas9 genome editing experiments and screens. *Nucleic Acids Res* **46**, W242-W245, doi:10.1093/nar/gky354 (2018).
22 Gu, B., Posfai, E., Gertsenstein, M. & Rossant, J. Efficient Generation of Large-Fragment Knock-In Mouse Models Using 2-Cell (2C)-Homologous Recombination (HR)-CRISPR. *Curr Protoc Mouse Biol* **10**, e67, doi:10.1002/cpmo.67 (2020).

23 Posfai, E. *et al.* Position- and Hippo signaling-dependent plasticity during lineage segregation in the early mouse embryo. *Elife* **6**, doi:10.7554/eLife.22906 (2017).

Figure legends:

Figure 1: Characterization and validation of C-YAP reporter in preimplantation embryos: A. Live imaging of C-YAP localization in preimplantation embryos. B. Immunofluorescence images of the C-YAP reporter (emiRFP670 fluorescence), endogenous YAP protein (Immunofluorescence) and CDX2 protein (Immunofluorescence) in a mouse blastocyst, showing perfect colocalization of YAP and CDX2 in the embryo. C. Manipulation of YAP-emiRFP670 localization by expressing a dominant-negative LATS2. Left: A schematic for mRNA injection experiment. mRNAs of H2B-RFP(the control group) or H2B-RFP+dnLATS2(the experiment group) were injected into one of the two cells of a 2-cell stage mouse embryo and then cultured to early blastocyst stage for analysis. Right upper panel, a control embryo shows that the expression of H2B-RFP did not cause nuclear YAP localization and CDX2 expression. Right bottom panel, a dnLATS2 injected embryo showed nuclear YAP and CDX2 expression in inside cells. Cells of interest were circled by dotted lines. D. Manipulation of YAP-emiRFP670 localization by treating with the ROCK inhibitor Y27632. Left: A schematic for the treatment experiment. Right, Snapshots from live imaging series Movie 1 showing ROCK inhibitor treatment leads to cytoplasmic Yap localization in embryos.

Figure 2: Dynamic YAP localization in 8-16 cell mouse embryos: A. Snapshots from live imaging series (Movie 3) as examples of YAP behavior in mitotic pairs. For the pair annotated by arrows, both cells presented nuclear YAP after the cell division at 80 mins,

and both of them located on the outside of the embryo and maintained nuclear YAP at 340 min. For the pair annotated by arrowheads, both cells presented nuclear YAP after the cell division at 80 min. Subsequently one of them was located on the outside of the embryo and maintained nuclear YAP while the other moved to the inside and presented cytoplasmic YAP at 340 min. (Quantitative data in extended figure 3B-D). B. Snapshots from live imaging series (Movie 4) with C-YAP embryos treated with the ROCK inhibitor Y-27632. During the 8-cell stage, 0 min to 630min, ROCK inhibition resulted in primarily cytoplasmic localization of Yap. After cell division, as demonstrated by the cell pair marked by arrows at 720min, all cells showed a transient nuclear localization of Yap. Then all cells gradually reversed to a cytoplasmic YAP localization status over time (810 min and 1170 min).

Extended Figure 1: Design and sequence of the YAP-C allele. A. Sequence of the guide RNA and structure of the repair donor. B. Exact sequence of the KI insert and homology arms confirmed by Sanger sequencing.

Extended Figure 2: Supplementary to the live imaging analysis of 8-16 cell transition of mouse embryos. A. Viable blastocysts after a live imaging session. B. Examples of the trends of nuclear YAP fluorescence intensity after cell division during live imaging. C. Statistical analysis of nuclear YAP fluorescence intensity in each mitotic pair right after cell division (0 min) and after 240 min (Each dot represents a cell, n=15. Bars present mean and 95% confident interval (CI). Left, mitotic pairs that present out-out pattern.

Right: mitotic pairs that present out-in pattern. D. Numeric analysis of cell division pattern within each embryo. Left, percentage of out-in and out-out patterned mitotic pairs in each embryo(n=23). Right, statistical analysis of percentage out-in pattern among all analyzed embryos(n=23). Presented as Mean and 95% CI. Actual mean=57.48%, one-sample t-test with the theoretical mean =50%, p=0.0381.

Extended Figure 3: Live imaging of Yap in early organogenesis stage embryos: A. Tile scan images of C-YAP embryos at three developmental stages: E8.0 (before turning), E8.5 (after turning), and E9.5. B. Zoom-in views of square marked regions in the E8.0 embryo: 1. Head fold, 2. Heart tube and 3. Neural tube. C. Zoom-in views of the somite region in the E8.5 embryo (square in image). D. Zoom in views of the limb bud region in the E9.5 embryo (square in image). Arrows in B-D mark examples of cells with strong nuclear Yap.

Movie legends:

Movie 1. Time lapse imaging of ROCKi treated YAP-emiRFP670 reporter embryos. Embryos were treated with 20μM and live imaged for 20 hours at a frame rate of 90min/frame.

Movie 2. Movie 2 Time lapse imaging YAP-emiRFP670 embryos from 8-16 cell stage. 8-cell stage YAP-emiRFP670 homozygous embryos were live imaged for 20 hours at a frame rate of 20min/frame.

Movie 2. Time lapse imaging YAP-emiRFP670 embryos from 8-16 cell stage. 8-cell stage YAP-emiRFP670 homozygous embryos were live imaged for 20 hours at a frame rate of 20min/frame.

Movie 3. Zoomed-in views of time lapse imaging of a single YAP-emiRFP670 embryos from 8-16 cell stage.

Movie 4. Time lapse imaging YAP-emiRFP670 embryos from 4-16 cell stage. Late 4-cell stage YAP-emiRFP670 homozygous embryos were live imaged for 28 hours at a frame rate of 20min/frame.

Movie 5. Movie 5 Zoomed in views of time lapse imaging of a single YAP-emiRFP670 embryo treated with ROCK inhibitor, illustrating that the initial YAP nuclear translocation after cell division was not affected by ROCK inhibition.

Movie 6. Rotational views of a live E8.0 (before turning) YAP-emiRFP670 embryo

Movie 7. Rotational views of a live E8.5 (after turning-10-somites stage) YAP-emiRFP670 embryo.

Movie 8. Rotational views of a live E9.5 YAP-emiRFP670 embryo.

Movie 9. Movie 9 Z-stak views of the head region of a E8.5 YAP-emiRFP670 embryo at 10-somites stage.

Movie 10. Time lapes imaging of the head region of a E8.5 YAP-emiRFP670 embryo at around 10-somites stage, illustrating a population of migrating cells that presented strong nuclear YAP signaling.

Figure 1

A

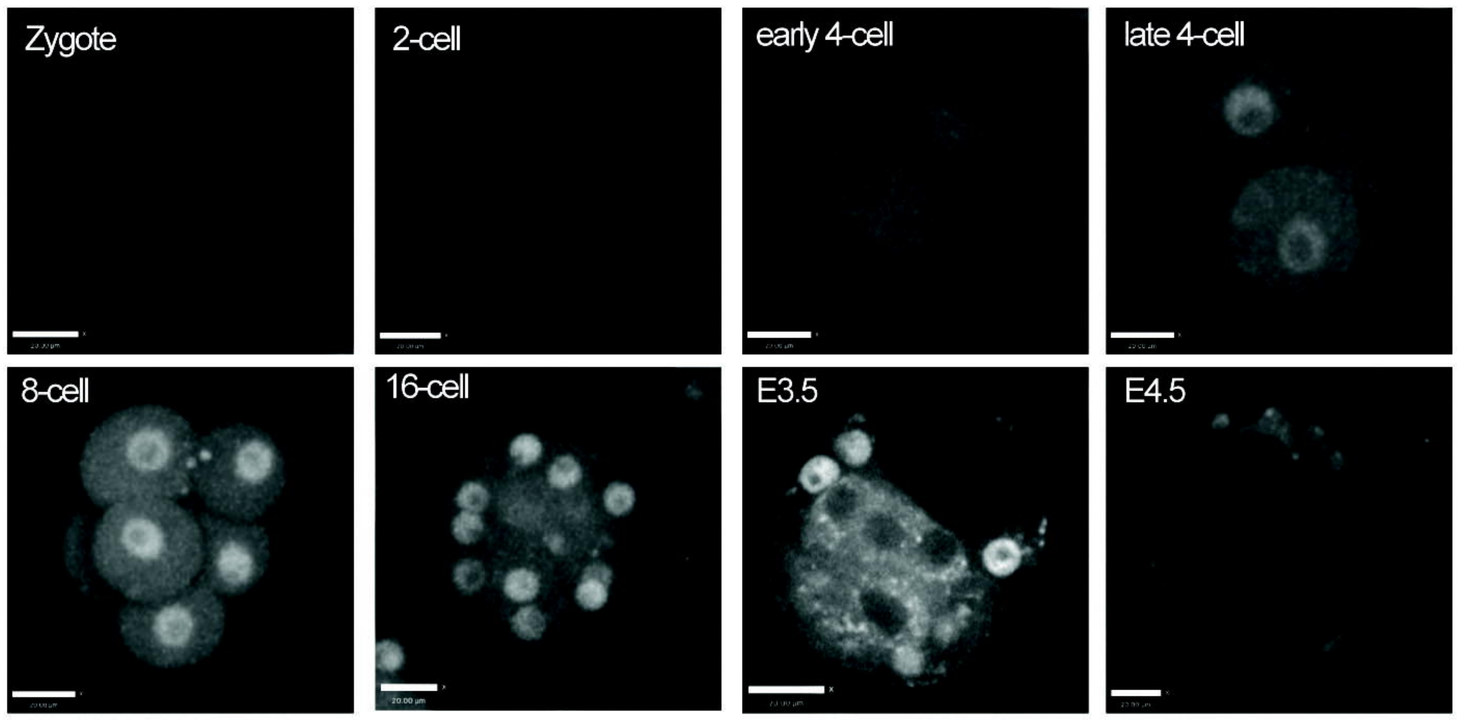

B

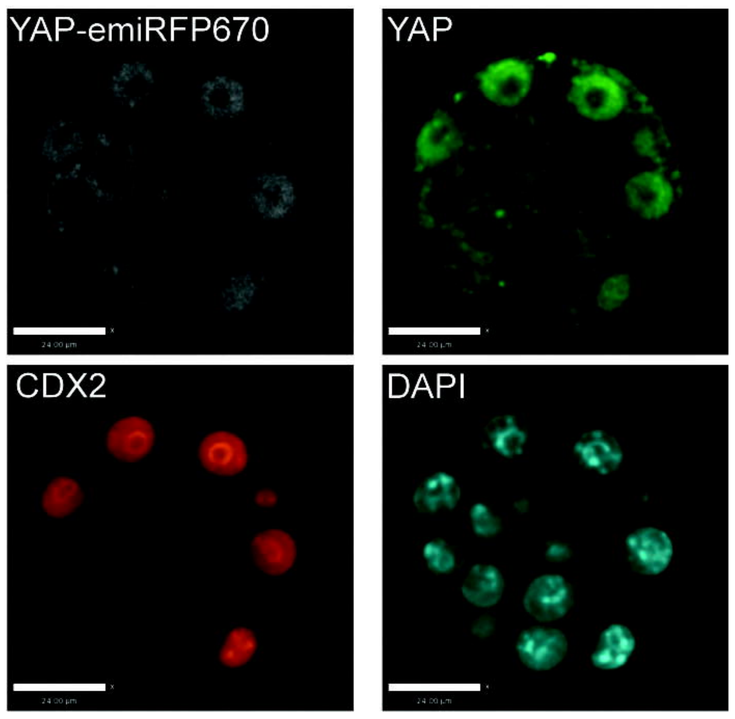

C

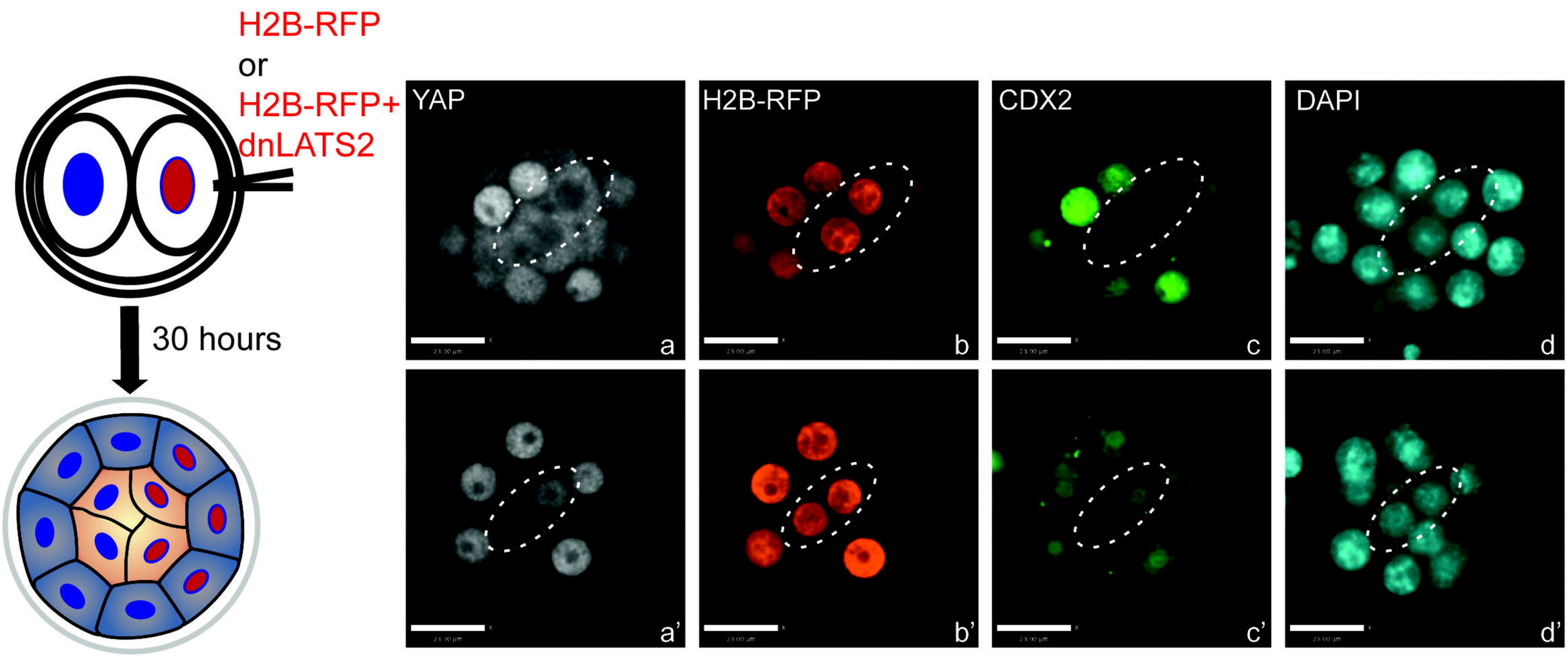

D

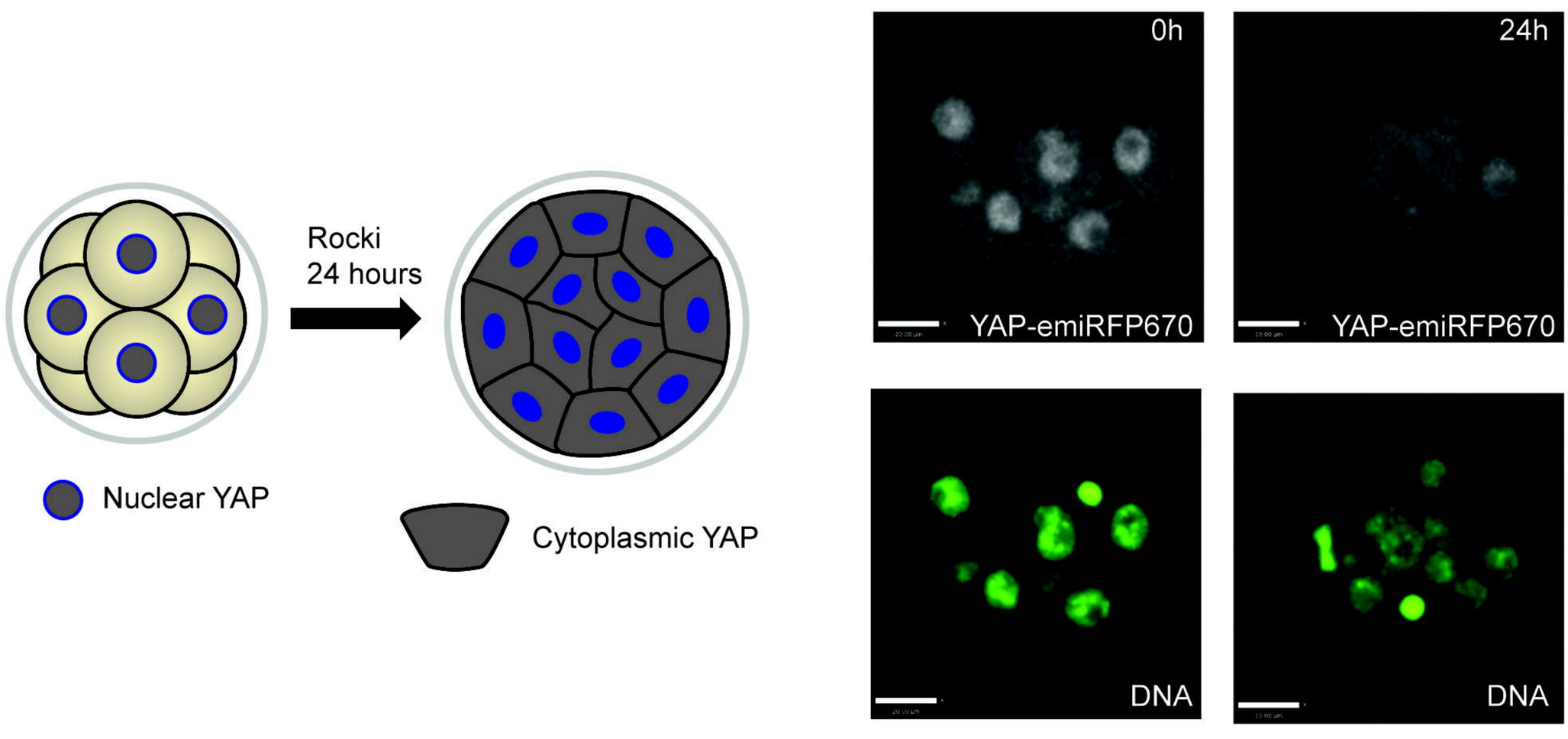

Figure 2

A

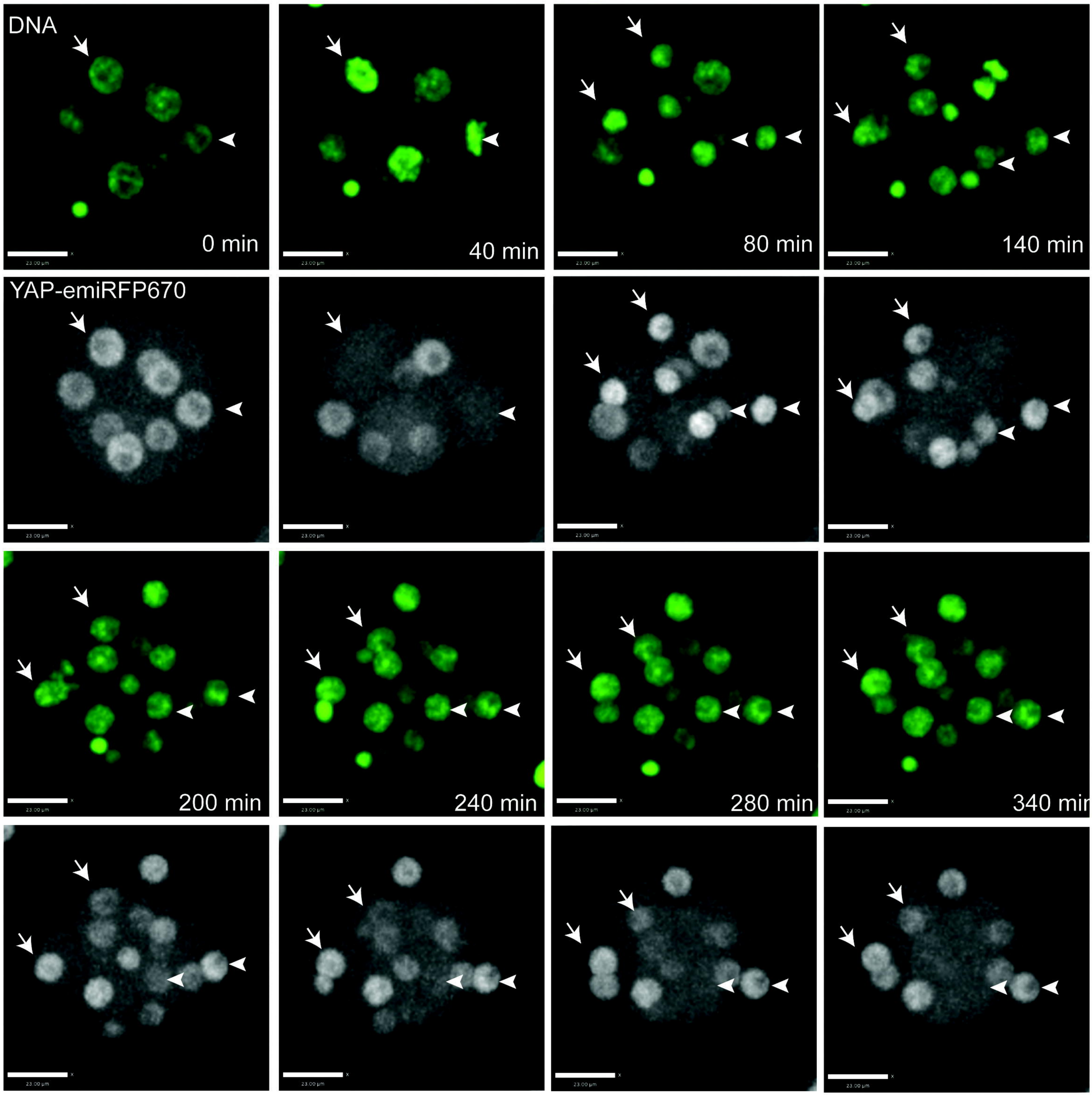
DNA
0 min
40 min
80 min
140 min
YAP-emiRFP670
200 min
240 min
280 min
340 min

B

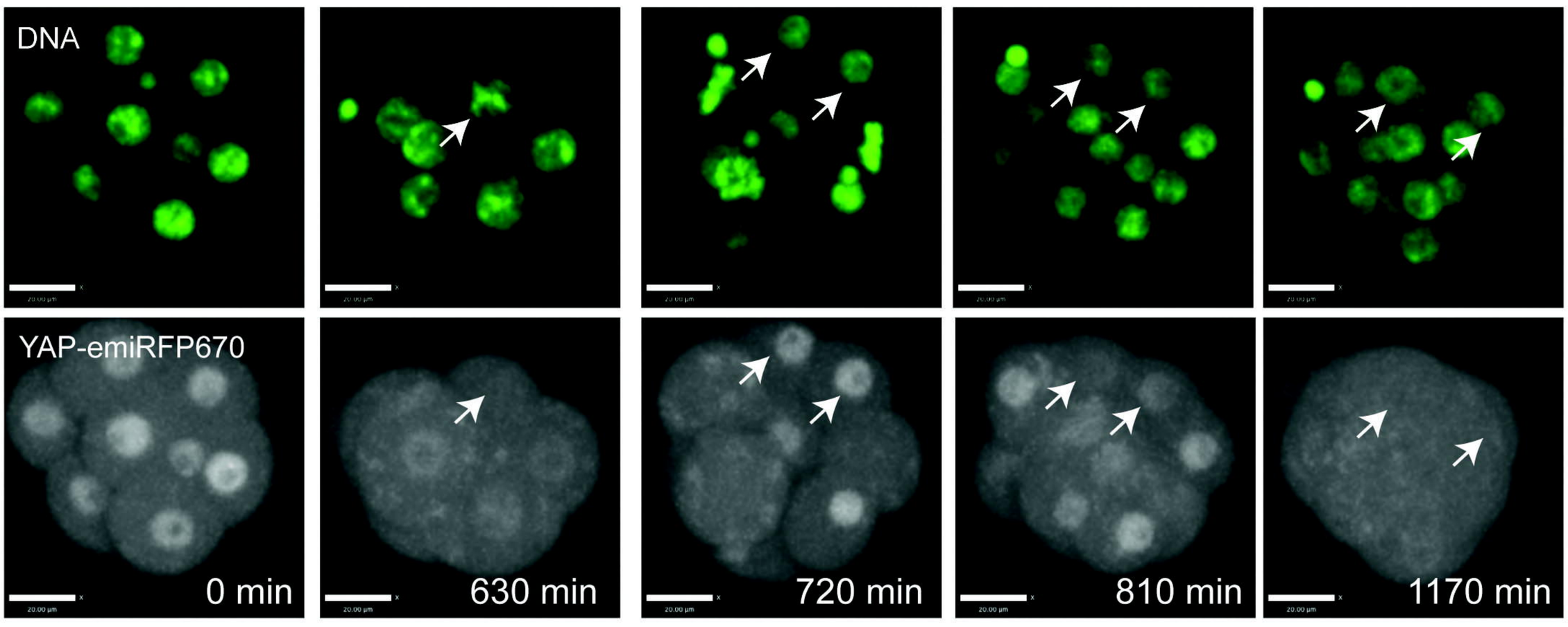
DNA
YAP-emiRFP670
0 min
630 min
720 min
810 min
1170 min

Extended Figure 1

A

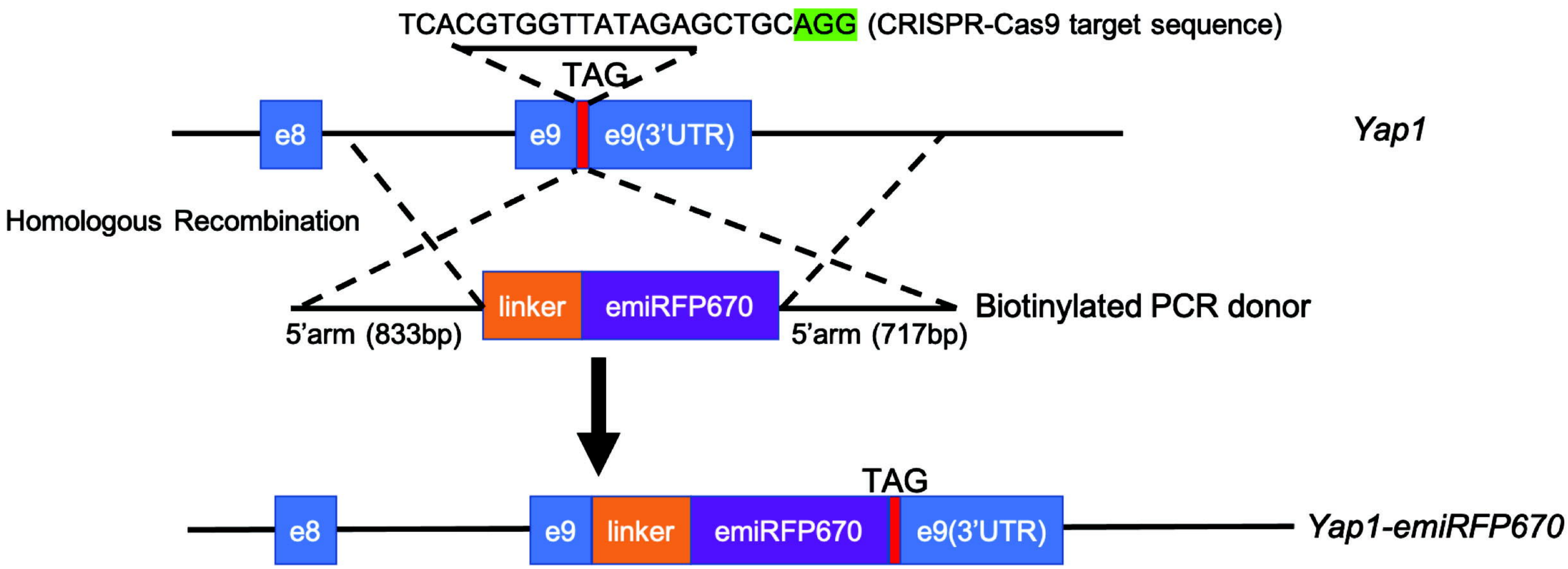

B

GTTCTAAGGTAGACACTGTGTGCTTCAGTTGCTGTGGGTATAGCTACGCTCACACAGGCAGCTCTGACACTGTGTGCTTCAGTTGCTATGGGT
ATAGCTACGCTCACACAGGCAGCTCTGACACTGTGTGCTTCAGTTGCTATGGGTATAGCTACGCTCACACAGGCAGCTCTGACGCTGTGTGCT
TCAGTTGCTGTGGGTATAGCTACGCTCACACAGGCAGCTCTGACACTGTGTGCTTCAGTTGGTATGGGTATAGCTACGCTCACACAGGCAGCT
CTGACACTGTGTGCTTCAGTTGGTATGGGTATAGCTATGCTCACACAGGCAGCTCTGACACTGTGTGCTTCAGTTGGTATGGGTATAGCTATG
CTCACACAGGCAGCTCTGACACTGTGTGCTTCAGTTGGTATGGGTATAGCTACGCTCACACAGGCAGCTCTGACACTGTGTGCTTCAGTTGGT
ATGGGTATAGCTACGCTCACACAGGCAGCTCTGACACTGTGTGCTTCAGTTGGTATGGGTATAGCTACGCTCACACAGGCAGCTCTGACACTG
TGTGCTTCAGTTGGTGTGGGTATAGCTACGCTCACACAGGCAGCTCTGACGCTTCTCACAGAACATTTGTTCATCCCTCCTCAAAACTAGGAGA
CACCATCAGCCAAAGCACCCTGCCGTCACAGCAGAGCCGCTTCCCCGACTACCTGGAAGCCCTCCCTGGGACAAATGTGGACCTTGGCACACT
GGAAGGAGATGCAATGAACATAGAAGGGGAGGAGCTGATGCCCAGTCTGCAGGAAGCGCTGAGTTCCGAAATCTTGGACGTGGAGTCTGT
GTTGGCTGCCACCAAGCTAGATAAAGAAAGCTTTCTCACGTGGTTAACGCGTggaggtggtggatcaggtggaggaggttctggaggtggtggatcaggagga
ggtggttctggaggtggtggatcaggaggaagatctcgaACTAGTatggcggaaggatccgtcgccaggcagcctgacctcttgacctgcgaacatgaagagatccacctcgccggc
tcgatccagccgcatggcgcgcttctggtcgtcagcgaacatgatcatcgcgtcatccaggccagcgccaacgccgcggaatttctgaatctcggaagcgtactcggcgttccgctcgccg
agatcgacggcgatctgttgatcaagatcctgccgcatctcgatcccaccgccgaaggcatgccggtcgcggtgcgctgccggatcggcaatccctctacggagtactgcggtctgatgc
atcggcctccggaaggcgggctgatcatcgaactcgaacgtgccggcccgtcgatcgatctgtcaggcacgctggcgccggcgctggagcggatccgcacggcgggttcactgcgcgcg
ctgtgcgatgacaccgtgctgctgtttcagcagtgcaccggctacgaccgggtgatggtgtatcgtttcgatgagcaaggccacggcctggtattctccgagtgccatgtgcctgggctcga
atcctatttcggcaaccgctatccgtcgtcgactgtcccgcagatggcgcggcagctgtacgtgcggcagcgcgtccgcgtgctggtcgacgtcacctatcagccggtgccgctggagccg
cggctgtcgccgctgaccgggcgcgatctcgacatgtcgggctgcttcctgcgctcgatgtcgccgtgccatctgcagttcctgaaggacatgggcgtgcgcgccaccctggcggtgtcgct
ggtggtcggcggcaagctgtggggcctggttgtctgtcaccattatctgccgcgcttcatccgtttcgagctgcgggcgatctgcaaacggctcgccgaaaggatcgcgacgcggatcacc
gcgcttgagagcTAGAGCTGCAGGGAGCCACTCTGAGTCTGTGAGGGATCCACAGAGCCTAAGATGTGCACGCCTGAAATTCAGATAAGTCAGT
GGGGGTTCTCTGGCTAACACAGAAAACAGATGAACCAGTGTCCATCGTTGTTCCGCTTTTCTCTGCCCGTCGCTGCTCTTACGTTGGTTGCTGA
CCTCTTCACGGCCGGCTCTAAAGAACCCGAACCGCAGACAGATTCCTTTGTTAACTCTGCTATGATAACTACGTTCTCTGGGATTGCTGGGGG
ATGGCCTGCTGGATAATGGATGTTCTGCCTTTTGTCCGGTGGTCCTTTCACCATCACTTTAACTGAACACACAGACTGGGAACTGAATGCTCTA
GAACATTGTTCAAGAGGTGGTTTCTTCAGCTGCCTTGGGTCCAACAAGCCAGAGGCATTGCGTCTGATCTCGTGGAGGACGGAGGGGACCCA
CGCTGAAGACTGGTGAACTTTCCATTCTTCTGTTAGCGATGCCGTTAGGCCATAGTGACCTGGGTCTTATCTTAGACGCTTATGAGGCATGAG
ACAGCTTCCATAGAAATATATTAATTATTACCACATACTCTAGATTAGGTTTGAATGAATATTTTCTGTGGGTGTTTTGGTTGGTTTTTCTCTGC
CCCCCCCCCCTTTTTTGTGGTTGGTCTTGGTGGAACGTAGGCAAATTAATGAATTCGTTTATAGCTGTAGCTTGGGGTGGGCAATACCATTCTT
TTGGTGGGAAATCTGTATTTCTTGGTTTTTTAACATCCTATTTAAATCTTAAATCTTGGTTATCTCCTCTCTACATATATACACACTCTTATTATGT
CTATGGTAGTGTGATAGCAGAATATATCTTTATAAACATTTCTTTCCTTTCCAGTTTATTTTTTAAATGGTAGCCTTGAACATATACATTTAGACA
CAGTAGTTTATGTTTCACAAATACTTTAAATTCTGGTTGGAGCAATTGCAGGTGTTTGAGGGAG

Upstream primer for sequencing
5' homology arm
30 amino acid linker translate to: GGGGSGGGGSGGGGSGGGGSGGGGSGGRSR
emiRFP670
5' homology arm
Downstream primer for sequencing

Extended Figure 2

A

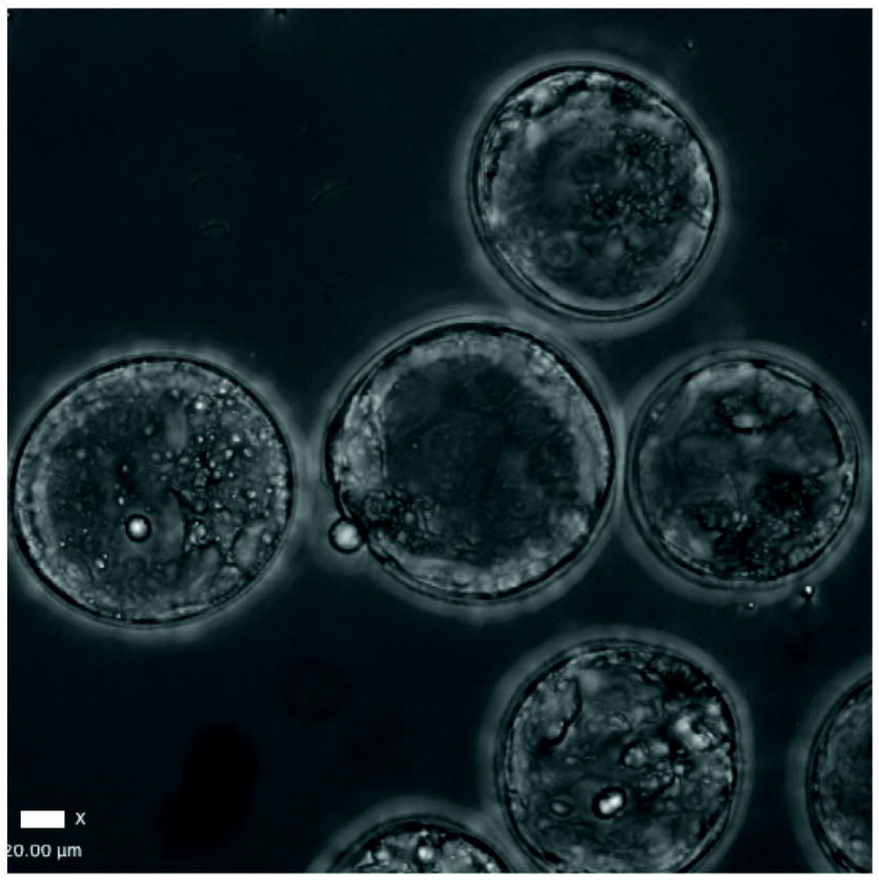

B

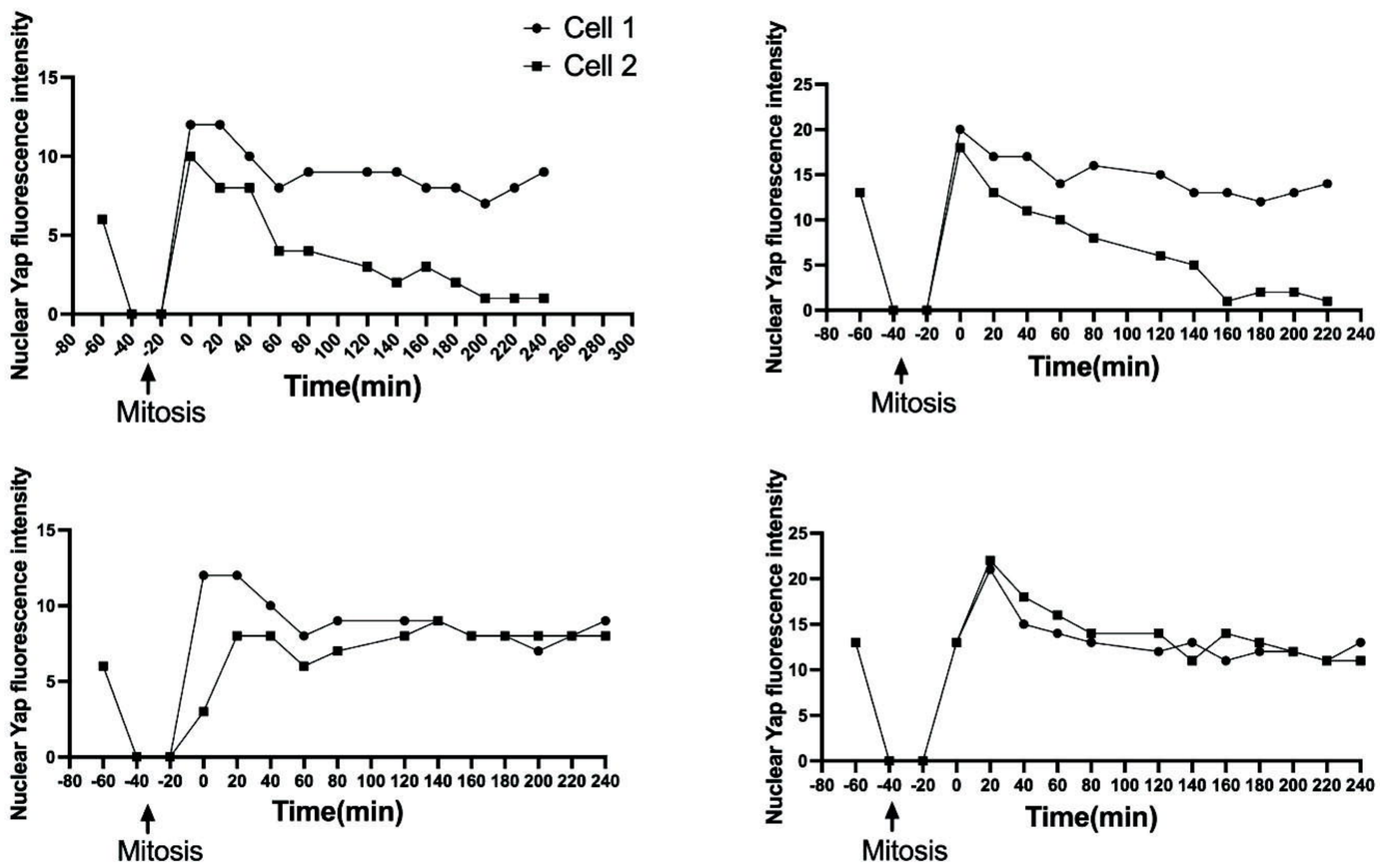

C

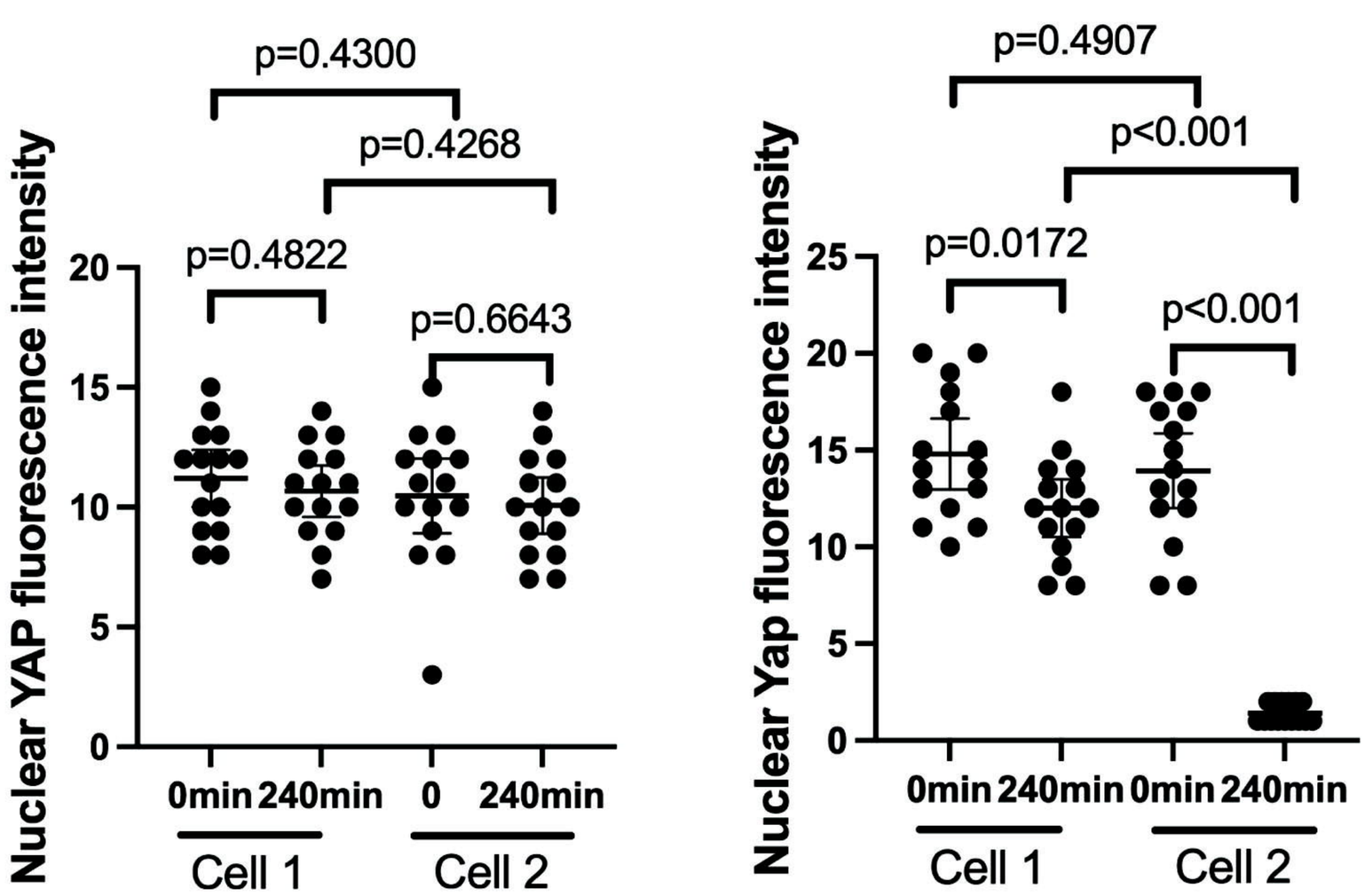

D

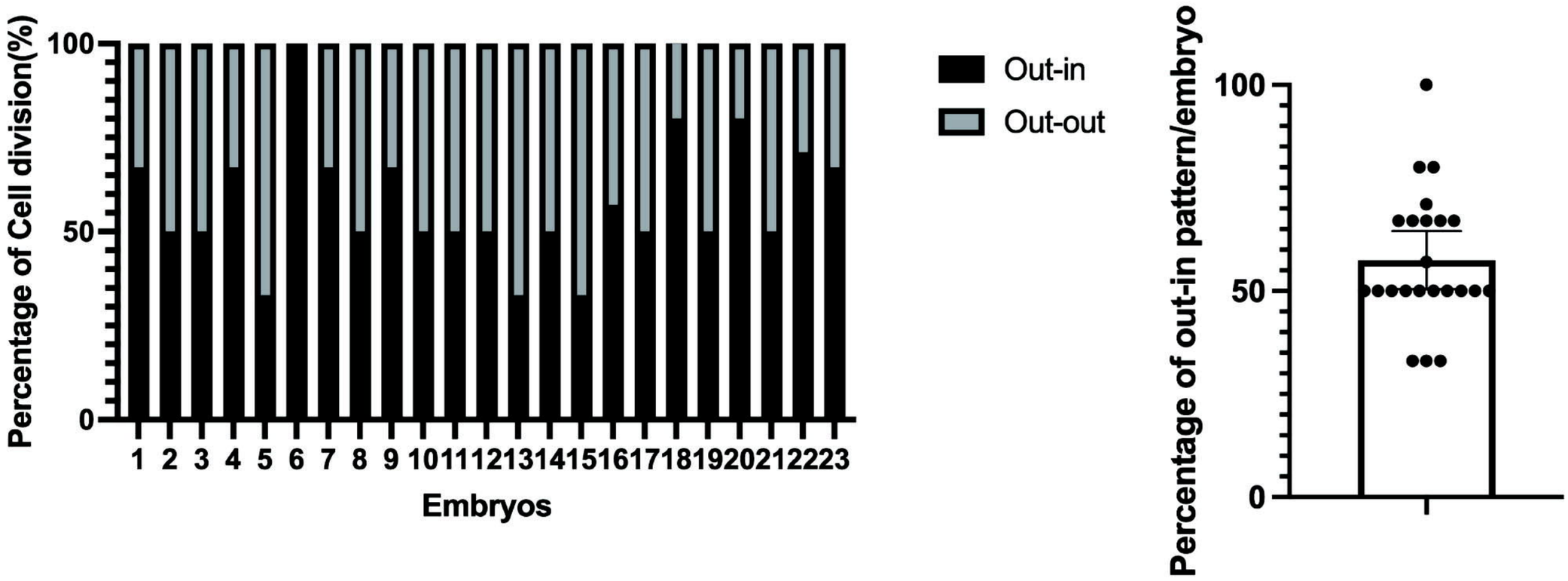

Extended Figure 3

A

E8.0

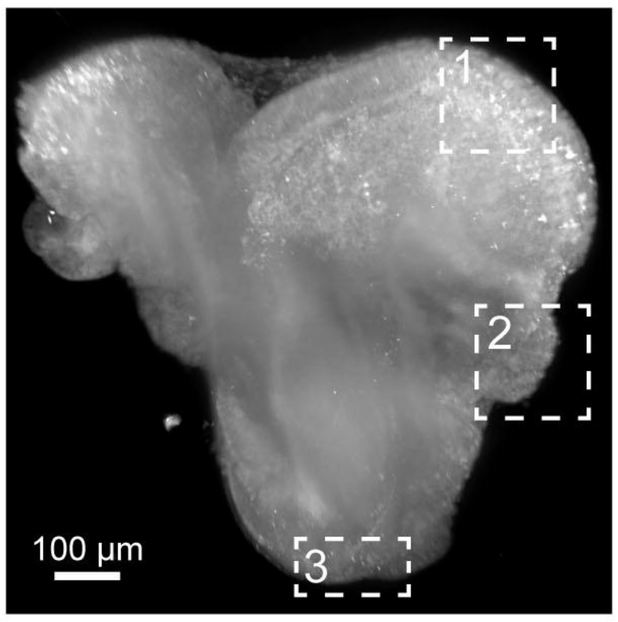

E8.5

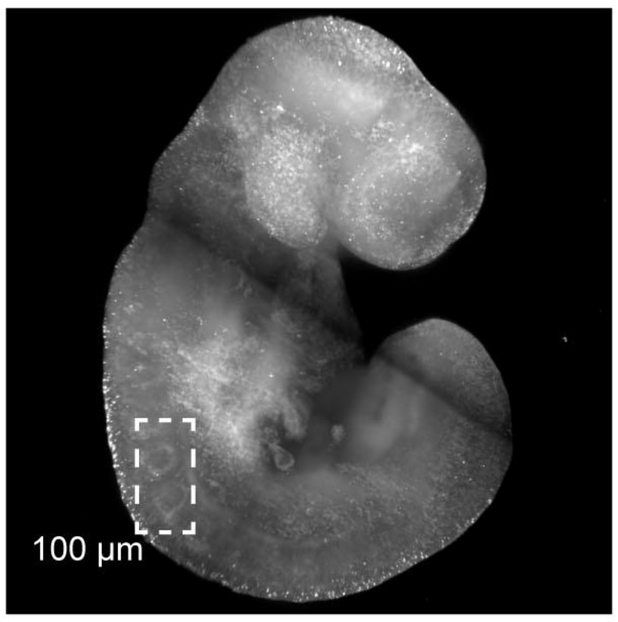

E9.5

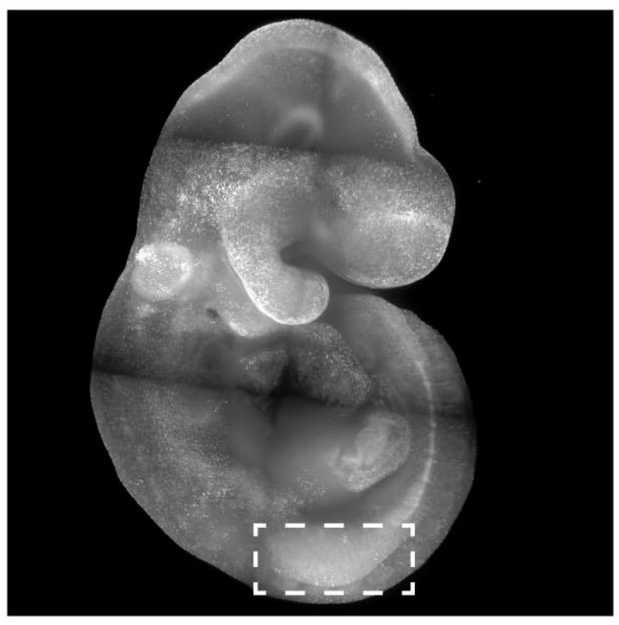

B

1. E8.0 Head (sagittal view)

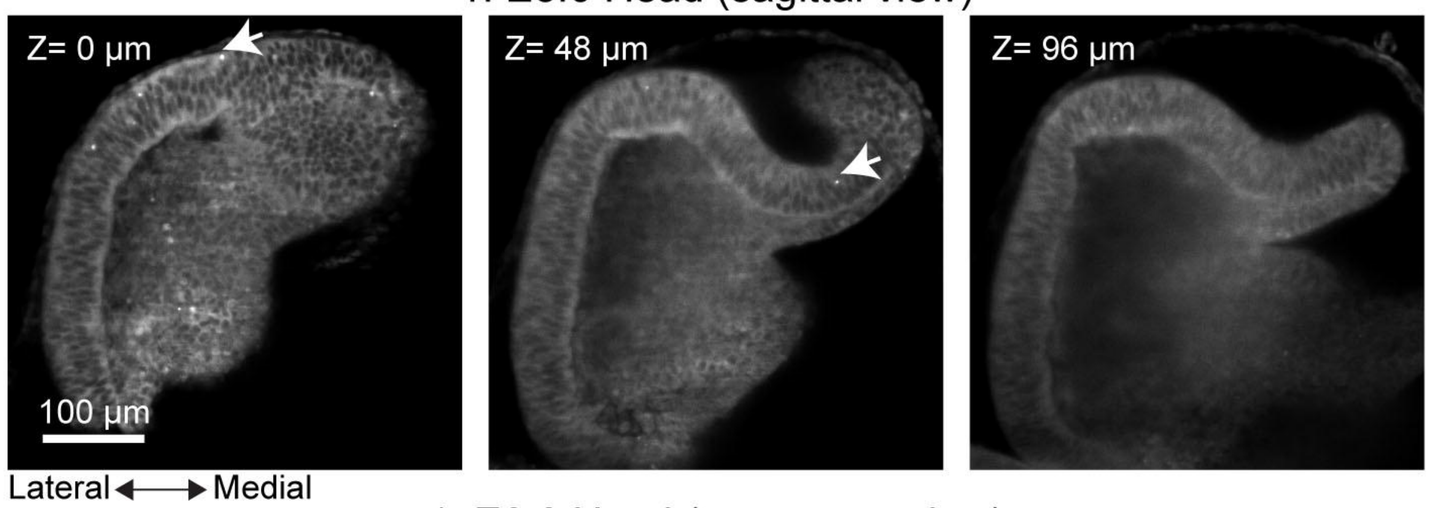

1. E8.0 Head (transverse view)

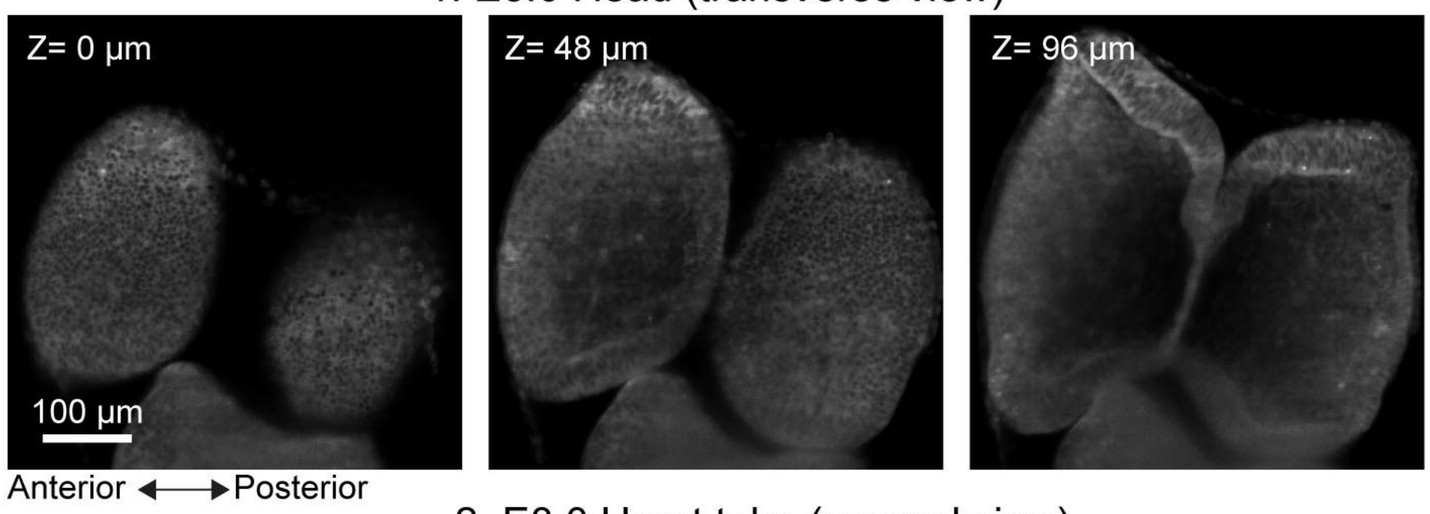

2. E8.0 Heart tube (coronal view)

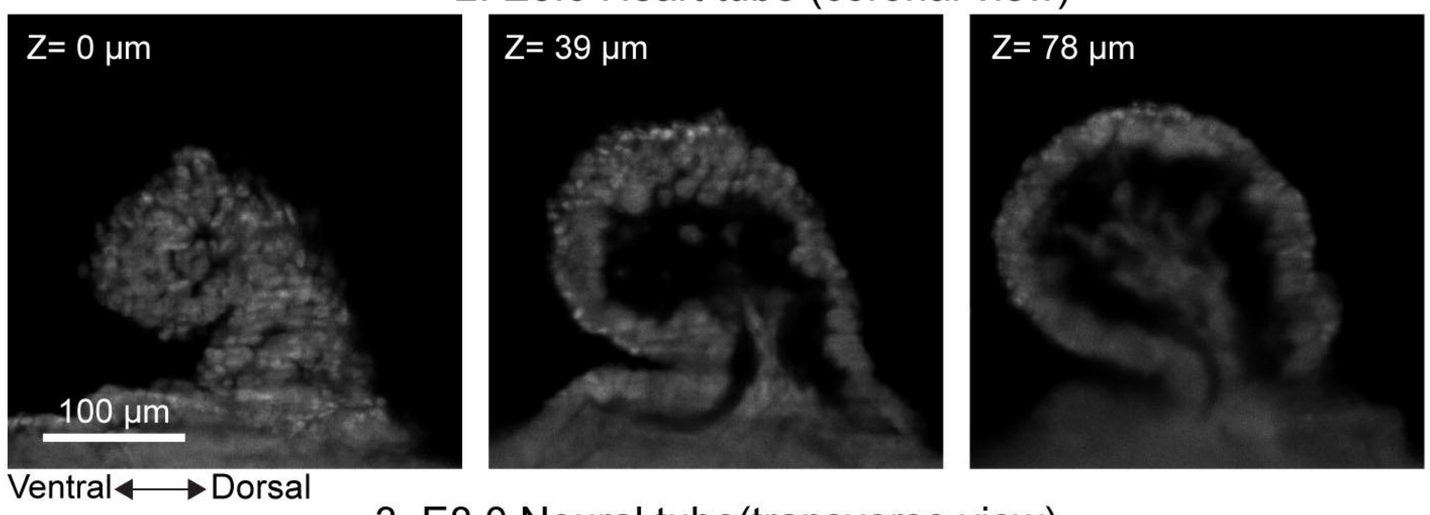

3. E8.0 Neural tube(transverse view)

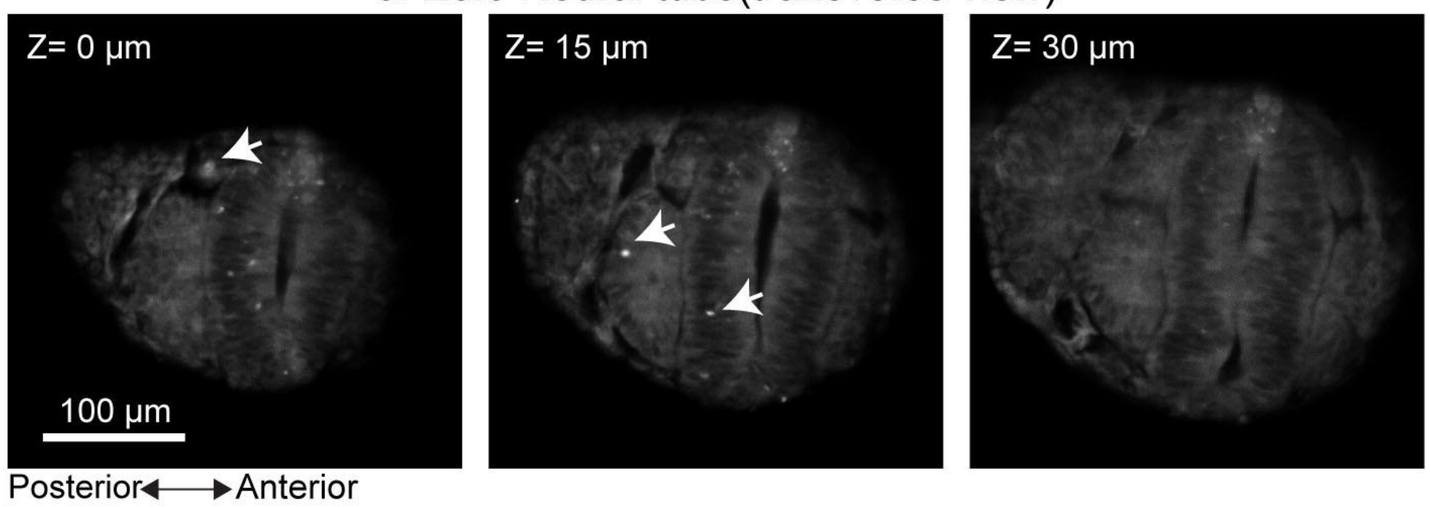

C

E8.5 somite (sagittal view)

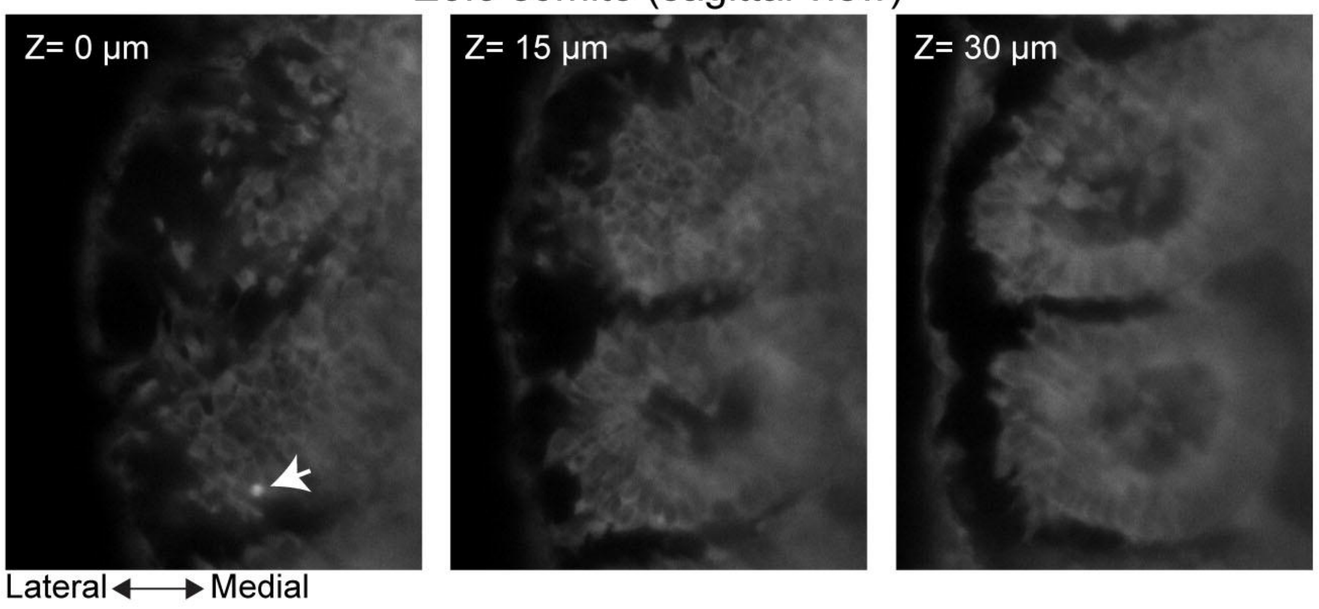

D
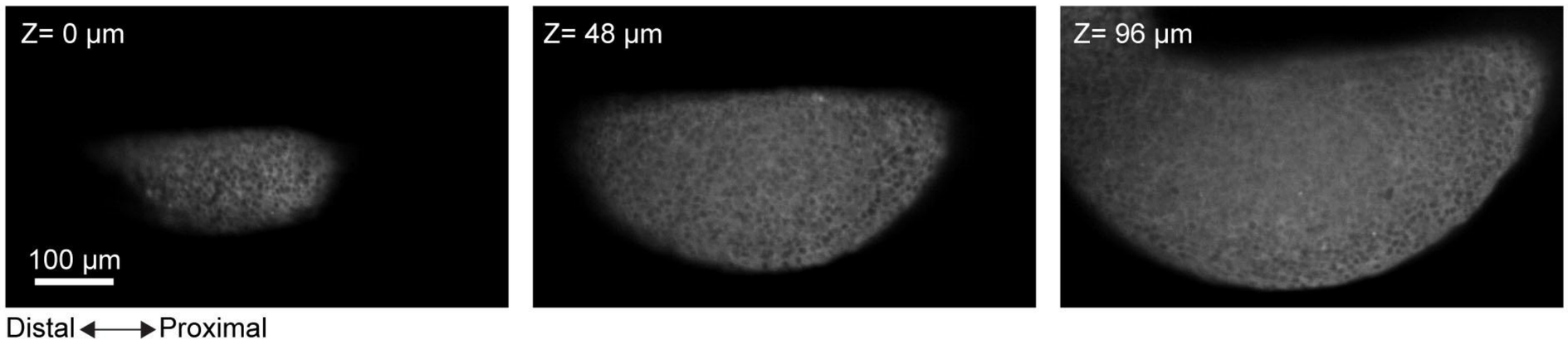
E9.5 forelimb bud (sagittal view)